Chemical Science

ROYAL SOCIETY OF CHEMISTRY

EDGE ARTICLE

View Article Online
View Journal | View Issue

Cite this: *Chem. Sci.*, 2021, **12**, 14207

All publication charges for this article have been paid for by the Royal Society of Chemistry

Attaining record-high magnetic exchange, magnetic anisotropy and blocking barriers in dilanthanofullerenes†

Sourav Dey and Gopalan Rajaraman *

While the blocking barrier (U_{eff}) and blocking temperature (T_B) for "Dysprocenium" SIMs have been increased beyond liquid N_2 temperature, device fabrication of these molecules remains a challenge as low-coordinate Ln^{3+} complexes are very unstable. Encapsulating the lanthanide ion inside a cage such as a fullerene (called endohedral metallofullerene or EMF) opens up a new avenue leading to several Ln@EMF SMMs. The *ab initio* CASSCF calculations play a pivotal role in identifying target metal ions and suitable cages in this area. Encouraged by our earlier prediction on $Ln_2@C_{79}N$, which was verified by experiments, here we have undertaken a search to enhance the exchange coupling in this class of molecules beyond the highest reported value. Using DFT and *ab initio* calculations, we have studied a series of $Gd_2@C_{2n}$ ($30 \leq 2n \leq 80$), where an antiferromagnetic $J_{Gd\cdots Gd}$ of -43 cm^{-1} was found for a stable $Gd_2@C_{38}$-D_{3h} cage. This extremely large and exceptionally rare 4f···4f interaction results from a direct overlap of 4f orbitals due to the confinement effect. In larger cages such as $Gd_2@C_{60}$ and $Gd_2@C_{80}$, the formation of two centre-one-electron (2c-1e$^-$) Gd–Gd bonds is perceived. This results in a radical formation in the fullerene cage leading to its instability. To avoid this, we have studied heterofullerenes where one of the carbon atoms is replaced by a nitrogen atom. Specifically, we have studied $Ln_2@C_{59}N$ and $Ln_2@C_{79}N$, where strong delocalisation of the electron yields a mixed valence-like behaviour. This suggests a double-exchange (B) is operational, and CASSCF calculations yield a B value of 434.8 cm^{-1} and resultant J_{Gd-rad} of 869.5 cm^{-1} for the $Gd_2@C_{59}N$ complex. These parameters are found to be two times larger than the world-record J reported for $Gd_2@C_{79}N$. Further *ab initio* calculations reveal an unprecedented U_{cal} of 1183 and 1501 cm^{-1} for $Dy_2@C_{59}N$ and $Tb_2@C_{59}N$, respectively. Thus, this study offers strong exchange coupling as criteria for new generation SMMs as the existing idea of enhancing the blocking barrier *via* crystal field modulation has reached its saturation point.

Received 19th July 2021
Accepted 6th October 2021

DOI: 10.1039/d1sc03925c

rsc.li/chemical-science

Introduction

Single molecule magnets (SMMs) are of prime interest in molecular magnetism due to their potential application in memory storage devices, qubits, *etc.*1,2 The figure of merit of an SMM is determined by the blocking barrier for magnetisation reversal (U_{eff}) and blocking temperature (T_B), the temperature below which opening of magnetic hysteresis is observed. These U_{eff} and T_B values are generally very high for lanthanides, thanks to their strong spin–orbit coupling.[3–10] The enhancement of T_B as high as 80 K in "Dysprocenium" complexes was an important breakthrough, replenishing the hope for potential applications in information storage devices.[11–15] Among others, important bottlenecks that are likely to hamper the futuristic application of these SMMs are (i) enhancing the blocking temperature beyond 80 K (ii) obtaining molecules that are stable under ambient conditions so that fabrication can be attempted (iii) retaining their intriguing magnetic properties upon fabrication – many of the best transition metal SMMs failed these criteria.[16–21]

To address the first challenge, among other strategies that could help enhance the barrier height/blocking temperature is the quenching of quantum tunnelling of magnetisation (QTM), which is prevalent at low temperatures. If a robust magnetic exchange between two Ln^{3+} ions is induced, it can act as a perturbation to reduce the degeneracy of Kramers doublets (KDs). This quenches the QTM and gives rise to large U_{eff} and T_B values.[22–24] However, obtaining a large exchange coupling between two Ln^{3+} metal ions is a formidable task as 4f orbitals are deeply buried, leading to a weak/no interaction in dinuclear or polynuclear Ln^{3+} complexes.[8,25–30]

In this regard, lanthanide encapsulated fullerenes (called endohedral metallofullerenes or EMFs) are gaining tremendous attention for various reasons: (a) they offer stability to guest molecules which are otherwise unstable;[31] (b) thanks to their

Department of Chemistry, Indian Institute of Technology Bombay, Powai, Mumbai 400076, India. E-mail: rajaraman@chem.iitb.ac.in

† Electronic supplementary information (ESI) available. See DOI: 10.1039/d1sc03925c

strong π cloud, fabrication of such molecules on graphene/HOPG/CNTs and other surfaces is straightforward;[31–39] (c) during this process guest molecules stay intact, and hence they are unlikely to lose their characteristics upon fabrication;[31] (d) as fullerenes are made of pure carbon, and the source of nuclear spin of the guest molecules can be controlled, they offer a nuclear spin free system – a key criterion for some qubit applications.[31,40] These key advantages mentioned here directly address the aforementioned goals (ii) and (iii), making them superior to traditional coordination chemistry/organometallic SMMs/SIMs.

One way to attain strong exchange coupling in lanthanide SMMs is to employ radical–Ln exchange which is substantially larger due to the direct exchange between 4f–2p orbitals.[41–43] In the search for a stronger exchange in Ln–radical systems, using a combination of DFT and *ab initio* methods, we have predicted a record high magnetic exchange coupling for a $Gd_2@C_{79}N$ radical fullerene complex and also suggested a very large blocking barrier for the Dy analogue.[44,45] Both these predictions were proved in a span of few years independently by two groups,[46–49] and $Gd_2@C_{79}N$ is found to have a very large spin relaxation time opening up a new avenue in spin-based qubits.[40,46] While a Ln–radical exchange could solve this problem,[41] the majority of the conventional lanthanide–radical systems are highly reactive and could pose a challenge in accomplishing the aforementioned goals (ii) and (iii).[41,43,50–55]

In this connection, if a robust exchange is induced between two Ln^{3+} ions, this will be very rewarding. One strategy to enhance the exchange coupling is to induce a weak Ln···Ln bond, which is possible if two ions are brought very close to each other directly. The metal–metal bonds in transition metal complexes are common but are scarce for lanthanides.[56–58] Inspired from the report that even noble gas elements such as He form He···He bonds under confinement, we devise such models for lanthanides that can offer very large 4f–4f exchange interactions.[59–63] In line with this idea, we have explored various $Gd_2@C_{2n}$ ($2n$ = 30–52, 60, 80) complexes in search of a stronger exchange and found $Gd^{3+}\cdots Gd^{3+}$ exchange as high as -43 cm^{-1}. In the second approach, we have extended our study to air-stable azafullerene radical analogues such as $Ln_2@C_{59/79}N$ (Ln = Gd, Tb, Dy). Using *ab initio* calculations, we have computed the double-exchange parameter B in these azafullerene cages. We have exploited the presence of double exchange to design SMMs based on Dy and Tb and unveil a new line of prediction with models exhibiting a U_{eff} value exceeding 1500 cm^{-1}.

Results and discussion

Achieving large exchange coupling in lanthanides is challenging as the 4f orbitals of lanthanides are deeply buried and interact weakly with ligand orbitals. The highest magnetic exchange between two Ln^{3+} ions is estimated in a $\{Gd_2Cr_2\}$ complex where J_{Gd-Gd} is +1.4 cm^{-1} ($\hat{H} = -J\hat{S}_1\hat{S}_2$).[28] As the Ln··· Ln distance plays a crucial role in controlling the 4f–4f exchange interaction, a large J is expected if two Ln^{3+} ions are confined in a fullerene cage. With this goal, we begin our study with Gd_2 endohedral fullerenes by varying the cage size from C_{30} to C_{80}. We have analysed the structure, binding energy, and magnetic properties within the DFT framework for two low energy conformers of the fullerene cages among various close-lying isomers.

Structure and bonding in $Gd_2@C_{2n}$ ($2n$ = 30–48, 52, 40, 80)

The C_{30} fullerene is the smallest cage where encapsulation leads to a stable geometry, as steric strain dominates over the metal-cage stabilisation in C_{28} and lower cages (Fig. 1, Table S1 and Appendix S1–S25†). For $Gd_2@C_{30}$, a C_{2v} isomer is found to be stable by 52.3 kJ mol^{-1} compared to the D_{5h} isomer due to stronger Gd–C interactions in the former as affirmed by the AIM analysis (see Table 1 for larger cages and Tables S1–S4 in the ESI†). In larger cages, the stability can be rationalised using (i) the number of APRs (Table S2†) and (ii) the nature of Gd–C interaction as obtained from the AIM analysis (see Fig. 1, S1–S26 and Tables S3–S27 in the ESI†).

Considering the Gd^{3+} ionic radius,[64] a Gd···Gd distance less than 2.5 Å (van der Walls radii) is likely to suggest a weak interaction or even a metal–metal bond. Such interactions are expected to reflect on J_{Gd-Gd} values with smaller values indicate weaker Gd···Gd interactions and not a metal–metal bond. Therefore, to compare the metal–metal interaction in $Gd_2@C_{2n}$ with $30 \le 2n \le 52$, the magnetic exchange J_{Gd-Gd} between two Gd^{3+} ions has been estimated using DFT calculations (B3LYP/TZV, $\hat{H} = -J\hat{S}_{Gd1}\hat{S}_{Gd2}$, see computational details and Table 1). The J_{Gd-Gd} is found to be antiferromagnetic in all $Gd_2@C_{2n}$ ($2n \le 52$) EMFs with the exception of $Gd_2@C_{44}$-C_s, $Gd_2@C_{48}$-C_{2v}, and $Gd_2@C_{52}$-D_{2d} EMFs having a ferromagnetic coupling (Table 1). The value in Table 1 suggests the decrease in antiferromagnetic interaction with the decrease in cage size. Within the same cage, the J_{Gd-Gd} value increases for a higher symmetry isomer. The largest antiferromagnetic J_{Gd-Gd} was estimated for $Gd_2@C_{30}$-D_{5h} (-62.7 cm^{-1}). This is several orders of magnitude larger than the experimentally known largest 4f–4f interaction. For the $Gd_2@C_{30}$-C_{2v} isomer, the J_{Gd-Gd} decreases to -49.6 cm^{-1} despite a shorter Gd···Gd distance compared to the D_{5h} isomer.

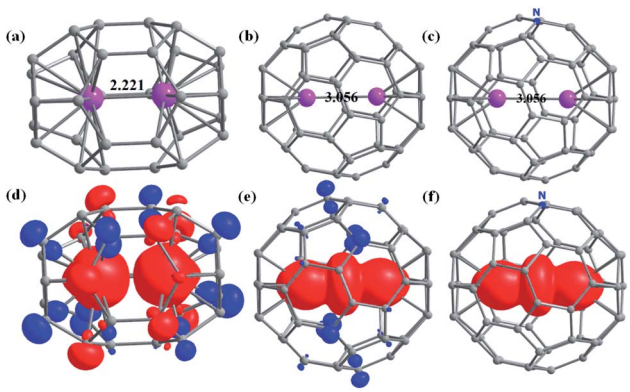

Fig. 1 The optimized structures of (and Gd–C bond length range) (a) $Gd_2@C_{30}$-D_{5h} (2.140–2.350 Å), (b) $Gd_2@C_{60}$-I_h (2.400–2.407 Å), and (c) $Gd_2@C_{59}N$-C_s (2.400–2.407 Å). The corresponding spin density plots for the high spin state are given in figures (d–f) with an isosurface value of 0.006 e$^-$ bohr^{-3}. Colour code: Gd-pink, C-grey, N-blue.

Table 1 The estimated J and the binding energy (kJ mol^{-1}) of chosen conformers in $Gd_2@C_{2n}$. Next to the symmetry label, the Gd⋯Gd distance is given in parentheses (Å). The value of spin density of each metal centre in the HS configuration of all $Gd_2@C_{2n}$ has been given below the exchange values in parentheses. All the J and B values are shown in cm^{-1}

$Gd_2@C_{2n}$	$J_{Gd\cdots Gd}$ (cm^{-1})		Binding energy (kJ mol^{-1})		ΔE (kJ mol^{-1})	
$2n = 30$	C_{2v} (2.185)	D_{5h} (2.224)	C_{2v}	D_{5h}	C_{2v}	D_{5h}
	$J_{Gd-Gd} = -49.8$ (6.96; 6.95)	$J_{Gd-Gd} = -62.7$ (6.94; 6.94)	1160.9	1149.8	0.0	52.3
$2n = 32$	C_2 (2.207)	D_3 (2.272)	C_2	D_3	C_2	D_3
	$J_{Gd-Gd} = -12.0$ (6.93; 6.95)	$J_{Gd-Gd} = -15.5$ (6.93; 6.93)	907.3	620.2	166.5	0.0
$2n = 34$	C_s (2.283)	C_2 (2.266)	C_s	C_2	C_s	C_2
	$J_{Gd-Gd} = -11.6$ (6.94; 6.94)	$J_{Gd-Gd} = -13.7$ (6.94; 6.94)	279.1	392.1	73.0	0.0
$2n = 36$	C_s (2.400)	D_{2d} (2.269)	C_s	D_{2d}	C_s	D_{2d}
	$J_{Gd-Gd} = -8.3$ (6.92; 6.97)	$J_{Gd-Gd} = -26.3$ (6.96; 6.95)	61.0	330.0	0.0	37.2
$2n = 38$	C_1 (2.443)	D_{3h} (2.734)	C_1	D_{3h}	C_1	D_{3h}
	$J_{Gd-Gd} = -7.0$ (6.97; 6.93)	$J_{Gd-Gd} = -43.4$ (6.99; 6.99)	−108.1	−63.0	0.0	478.1
$2n = 40$	C_{2v} (2.376)	D_2 (2.400)	C_{2v}	D_2	C_{2v}	D_2
	$J_{Gd-Gd} = -4.9$ (7.00; 7.00)	$J_{Gd-Gd} = -10.3$ (6.99; 6.99)	0.7	−173.2	320.6	0.0
$2n = 42$	C_1 (2.495)	D_3 (2.430)	C_1	D_3	C_1	D_3
	$J_{Gd-Gd} = -3.0$ (6.99; 6.99)	$J_{Gd-Gd} = -7.6$ (7.00; 7.00)	−337.3	−193.1	0.0	60.8
$2n = 44$	C_s (2.608)	D_2 (2.549)	C_s	D_2	C_s	D_2
	$J_{Gd-Gd} = 0.2$ (6.98; 7.02)	$J_{Gd-Gd} = -8.4$ (7.00; 7.00)	−386.9	−308.0	157.1	0.0
$2n = 46$	C_1 (2.728)	C_s (2.796)	C_1	C_s	C_1	C_s
	$J_{Gd-Gd} = -1.4$ (6.99; 7.00)	$J_{Gd-Gd} = -0.3$ (6.98; 6.98)	−494.8	−537.0	42.1	0.0
$2n = 48$	C_1 (2.836)	C_{2v} (3.002)	C_1	C_{2v}	C_1	C_{2v}
	$J_{Gd-Gd} = -0.4$ (7.00; 7.00)	$J_{Gd-Gd} = 0.7$ (6.99; 6.99)	−560.2	−534.3	0.0	410.6
$2n = 52$	C_s (3.282)	D_{2d} (2.324)	C_s	D_{2d}	C_s	D_{2d}
	$J_{Gd-Gd} = -1.3$ (7.02; 6.99)	$J_{Gd-Gd} = 2.7$ (7.04; 7.04)	−595.2	−991.4	224.3	0.0
$2n = 60^b$	$Gd_2@C_{60}$-I_h (3.056)	$Gd_2@C_{59}N$-C_s (3.056)	$Gd_2@C_{60}$-I_h	$Gd_2@C_{59}N$-C_s		
	$J_1 = 869.8, J_2 = 0.08, J_3 = 40.2$, $B = 434.8$ (7.53; 7.53)	$J_1 = 869.8, J_2 = 0.08$, $B = 434.8$ (7.54; 7.54)	−369.4[a]	−389.1[a]		
$2n = 80^b$	D_{5h} (3.818)	C_{2v} (4.074)	D_{5h}	C_{2v}	D_{5h}	C_{2v}
	$J_1 = 404.6, J_2 = 0.03, B = 202.1$, $J_3 = -41.3$ (7.54; 7.54)	$J_1 = 351.3, J_2 = 0.03$, $B = 175.6, J_3 = -95.5$ (7.52; 7.53)	−987.6[a]	−840.5[a]	0.0	96.7
$2n = 80^b$	$Gd_2@C_{79}N$-C_s-1 (3.816)	$Gd_2@C_{79}N$-C_s-2 (4.107)	$Gd_2@C_{79}N$-C_s-1	$Gd_2@C_{79}N$-C_s-2	$Gd_2@C_{79}N$-C_s-1	$Gd_2@C_{79}N$-C_s-2
	$J_1 = 404.6, J_2 = 0.03$, $B = 202.1$ (7.55; 7.55)	$J_1 = 351.3, J_2 = 0.03$, $B = 175.6$ (7.51; 7.53)	−958.0[a]	−733.7[a]	0.0	157.7

[a] The binding energy has been calculated with respect to electronic energy. In all other isomers, the binding energy has been calculated with respect to electronic and thermal free energies. [b] Here 'n' represents the total number of atoms, including the one nitrogen atom.

This is due to stronger 4f–4f overlaps (Tables S28–S29†). Although the Gd⋯Gd distances are very similar for C_{30} and C_{32}, the J_{Gd-Gd} value is significantly smaller in $Gd_2@C_{32}$ (see Table 1) due to symmetry constraints and the associated 4f–4f overlaps (see Tables S30–S49 in ESI†). Further increase in the cage size only nominally decreases the J_{Gd-Gd} values with several exceptions, though lower symmetry models follow the trend (see Fig. S27†). A net ferromagnetic interaction is observed in $Gd_2@C_{44}$-C_s, $Gd_2@C_{48}$-C_{2v} and $Gd_2@C_{52}$-D_{2d} cages due to a meagre contribution to the antiferromagnetic part of J (see Tables S42, S46 and S48†). Orbital orthogonality of 4f-orbitals and dipolar contributions due to shorter Gd⋯Gd distance leads to a net ferromagnetic coupling in these examples. A very large 4f–4f overlap suggests a possibility of direct 4f–4f interactions between two lanthanide ions, which are hard to observe in classical coordination chemistry. The binding energy becomes positive for $Gd_2@C_{2n}$ with $2n \leq 36$ and negative for $Gd_2@C_{2n}$ with $2n > 36$ (see Table 1) except for the $Gd_2@C_{40}$-C_{2v} isomer, where it is thermoneutral (0.7 kJ mol^{-1}). Thus, it suggests that the large antiferromagnetic interaction is feasible for the isomers of $Gd_2@C_{2n}$ with $2n > 36$.

The magnitude of the spin density of the two Gd^{3+} ions increases with an increase in ring size, supported by the contour plots of the electron density map obtained from AIM analysis (Fig. S28–S54 and Tables S50, S51†). Particularly a sudden jump in the magnitude of spin density is noted for $Gd_2@C_{60}$, with nearly one electron found between the two Gd ions (see Fig. 1, S50–S52†). Our NBO analysis reveals that this electron is delocalised in the formally empty orbitals, which are hybridised among 6s, 6p, and 5d orbitals ($6s6p^{0.11}5d^{0.33}$, see Fig. S55†). Thus, it suggests a strong valence delocalisation where one unpaired electron is delocalised to vacant 5d/6s/6p orbitals of each Gd^{3+} ion leading to a type-III class of mixed valence systems ($Gd^{2.5+}\cdots Gd^{2.5+}$, see later).[65]

Mechanism of the formation of $Gd_2@C_{2n}$

To further investigate the unusual behaviour wherein the cage size decides the magnitude of the spin density present between the Gd^{3+} ion, we have analysed the formation of $Gd_2@C_{2n}$ from the HOMO–LUMO gap perspective. In the formation of dimetallofullerene $Gd_2@C_{2n}$, we can presume that two Gd atoms donate three electrons each from their frontier orbitals (5d and

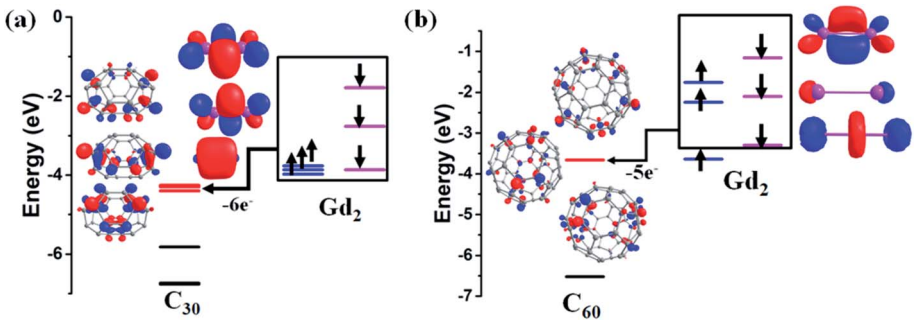

Fig. 2 The MO diagrams corresponding to the formation of (a) $Gd_2@C_{30}$-C_{2v} and (b) $Gd_2@C_{60}$-I_h isomers. The three black and red horizontal lines correspond to the energy of the occupied and empty orbitals of the C_{2n} fullerene ring, respectively. The blue and pink horizontal lines correspond to the energy of α and β orbitals of the Gd_2 fragment. We have shown the three lowest unoccupied α orbitals of the C_{2n} fullerene cage with an isosurface value of 0.055 e^- $bohr^{-3}$. The three highest occupied α orbitals for Gd_2 in the C_{30} and C_{60} fullerene cage are also shown (isosurface 0.06 e^- $bohr^{-3}$). Colour code: Gd-pink, C-grey.

6s orbitals) to the three lowest unoccupied molecular orbitals (LUMOs) of the C_{2n} cage resulting in $Gd_2^{6+}@C_{2n}^{6-}$.[66] Thus, the formation of $Gd_2@C_{2n}$ depends on the energy gap between the frontier orbitals of Gd_2 and the LUMOs of the C_{2n} cage. If the LUMOs of the C_{2n} cage are found to be lower in energy than the frontier orbitals of the Gd_2 fragment, a large stabilisation occurs after the electron transfer. Quite interestingly, this is the case for the C_{2n} cage with $2n \leq 52$, which favours the transfer of six electrons from Gd_2 (with the Gd–Gd distance <3.0 Å, ignoring 4f orbitals, the valence electron configuration is $\sigma_g^2\sigma_u^1\pi_g^1\pi_u^2$)[67] to the C_{2n} cage (Fig. 2a for $Gd_2@C_{30}$ and Fig. S56 and S57† for $Gd_2@C_{52}$-D_{2d} and $Gd_2@C_{48}$-C_{2v}). As the ring size increases, the LUMOs of the C_{2n} cage destabilised. In $Gd_2@C_{60}$ with the Gd⋯Gd distance of 3.056 Å, the bonding in the Gd_2 fragment before encapsulation is found to be $\sigma_g^2\pi_u^3\sigma_u^1$ (ignoring the 4f orbitals, Fig. 2b). After encapsulation, the five electrons are fully transferred to the cage except one σ_g^1 electron (here the β electron in Fig. 2b for $Gd_2@C_{60}$-I_h) resulting in a 2c-1e$^-$ bond between two Gd atoms. This is due to the comparable energy of the beta (6s/5d) σ_g^1 orbital with the LUMO of the C_{2n} cage.

Estimation of magnetic exchange in $Gd_2@C_{59}N$-C_s, $Gd_2@C_{79}N$-C_s-1, and $Gd_2@C_{79}N$-C_s-2

The most sensitive parameter that yields insight into the spin density distribution discussed in the last section is the corresponding exchange coupling J_{Gd-Gd}. Here we intend to compute this parameter and analyse this with respect to the cage size. The mechanism of formation of $Gd_2@C_{2n}$ suggests the presence of one unpaired electron between two Gd^{3+} ions and another conjugate electron in the fullerene cage for $Gd_2@C_{60}$-I_h, $Gd_2@C_{80}$-D_{5h}, and $Gd_2@C_{80}$-C_{2v} isomers (see Table S50†). For these molecules, a complex set of magnetic coupling emerges: (i) the coupling between Gd^{3+} and the radical that reside inside the cage (J_1), (ii) the second one describes the coupling between two Gd^{3+} ions (J_2), (iii) the third one describes the coupling between two radicals (J_3) and (iv) in addition to these isotropic exchange coupling values, a strong electron delocalisation of the radical between two Gd^{3+} ions suggests a double-exchange (parameter B) being operative between two Gd ions (in a fully delocalised case, $Gd_2^{2.5+}$). All these exchanges have been illustrated in Scheme S2.† This is similar to a type-III mixed-valence

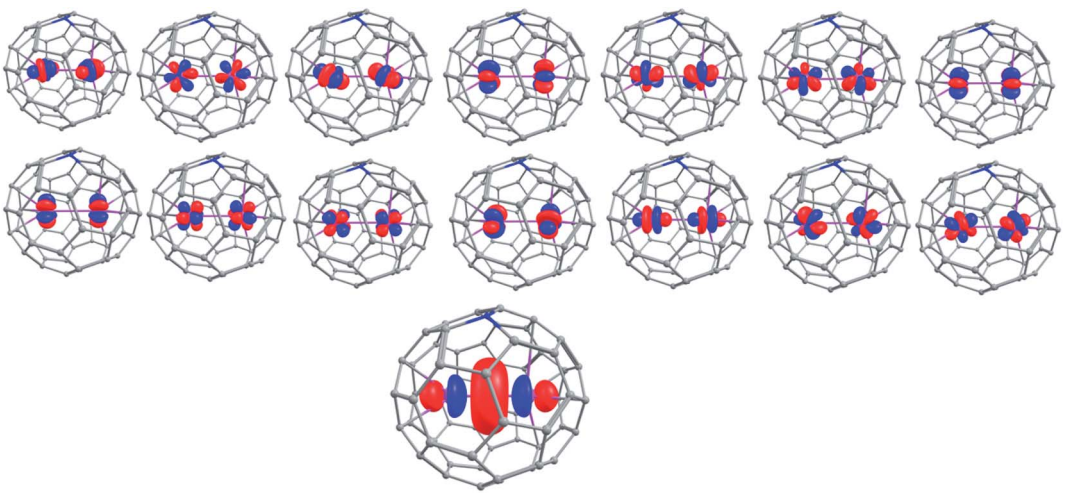

Fig. 3 The fifteen active orbitals of $Gd_2@C_{59}N$ with CAS (15,15) active space for the $S = 15/2$ state. Colour code: Gd-pink, C-grey, N-blue.

system[68,69] where the spin Hamiltonian parameters are estimated using the following Hamiltonian[70]

$$H = -J(S_A \cdot S_B \cdot O_A + S_A \cdot S_B \cdot O_B) + BT_{AB}, \quad (1)$$

where J and B denote the exchange interaction and delocalisation parameter, respectively, S_A and S_B are the total spin multiplicity of centres A and B, respectively, O_A and O_B are the localisation operator, and T_{AB} is the electron transfer operator (see computational details for more information).

The presence of one unpaired electron in the fullerene cage of $Gd_2@C_{60}$-I_h, $Gd_2@C_{80}$-D_{5h}, and $Gd_2@C_{80}$-C_{2v} leads to polymerisation or aggregation, and often, these complexes are not isolable.[71,72] There are two strategies available to demonstrate their existence (i) by transforming them into a chemically stable form with one-electron reduction/substitution at the ring position. This has been adapted to stabilise the $Dy_2@C_{80}$-I_h molecule by chemically transforming it to $Dy_2@C_{80}(CH_2Ph)$.[72–75] (ii) By substituting one of the carbon with the nitrogen atom yielding azafullerenes such as $Ln_2@C_{79}N$ and other analogues.[49,70,76–79] Here, we have adopted the second approach where one carbon atom is substituted by nitrogen in $Gd_2@C_{60/80}$ isomers yielding $Gd_2@C_{59/79}N$ molecules (see Appendix S26–S28† for optimised coordinates) possessing C_s symmetry (here $Gd_2@C_{79}N$-C_s-1 is derived from $Gd_2@C_{80}$-D_{5h} and $Gd_2@C_{79}N$-C_s-2 is derived from $Gd_2@C_{80}$-C_{2v}, see Table 1). Upon substitution, as expected, the spin density of the cage in $Gd_2@C_{59/79}N$ was seized (see Fig. 1e and f for the 665 isomer, see ref. 44). While $Gd_2@C_{79}N$ is a well-characterised and thoroughly studied molecule, $Gd_2@C_{59}N$ is not known. However, the X-ray structure of $C_{59}N$ and encapsulation of some metal ions are experimentally studied, and their existence has been proved beyond ambiguity.[35,80–86] Particularly, $K_6C_{59}N$ has been isolated and characterised thoroughly. This suggests that the $C_{59}N^{6-}$ cage is a stable molecular fragment and can encapsulate Ln^{3+} cations similar to those hypothesised here.[87–89]

This type-III mix valence moiety of $Gd_2@C_{59}N$-C_s, $Gd_2@C_{79}N$-C_s-1, and $Gd_2@C_{79}N$-C_s-2 isomer represents a multireference wave function as the unpaired electron is not localised on a particular centre. Therefore, a multireference method such as the state-average CAS(15,15)SCF set up was employed to estimate the double exchange parameter (B) (Fig. 3, see computational details).[90] As per the CASSCF calculations, the additional radical electron resides in a hybrid orbital containing coefficients from 6s, $5p_z$, $6p_z$, and $5d_{z^2}$ orbitals of Gd_1 and Gd_2 centres (see Table S55† for composition). The set of spin Hamiltonian parameters obtained from the CASSCF calculations are as follows, $Gd_2@C_{59}N$-C_s ($Gd_2@C_{79}N$-C_s-1) [$Gd_2@C_{79}N$-C_s-2]: J_1 = +869.8 (+404.6) [+351.3] cm^{-1}, J_2 = 0.08 (0.03) [0.03] cm^{-1} and B = +434.8 (+202.1) [+175.6] cm^{-1} (Table 1). For all three complexes, the J_1 interaction is found to be extremely large, and this is due to the involvement of the diffuse virtual 6s and $6p_z$ and $5d_{z^2}$ orbitals of Gd ions, while the J_2 coupling between two Gd^{3+} ions is found to be very small as the 4f orbitals are only weakly interacting here. It is worth mentioning that we have previously reported a very large J_1 value of +400 cm^{-1} ($\hat{H} = -J\hat{S}_1\hat{S}_2$) in $Gd_2@C_{79}N$ using the UB3LYP/TZV setup.[44] The estimated J_1 value by our *ab initio* approach for $Gd_2@C_{79}N$ lies in the range of 350–405 cm^{-1}, and this is in line with the DFT calculations and experimental reports (−350 ± 20 cm^{-1} using $\hat{H} = J_1(\hat{S}_{Gd_1}\hat{S}_{rad} + \hat{S}_{Gd_2}\hat{S}_{rad}) + J_2(\hat{S}_{Gd_1}\hat{S}_{Gd_2})$ in ref. 40 and a J_1 value of 170 ± 10 cm^{-1} using the Hamiltonian $\hat{H} = -2J_1(\hat{S}_{Gd_1}\hat{S}_{rad} + \hat{S}_{Gd_2}\hat{S}_{rad}) - 2J_2(\hat{S}_{Gd_1}\hat{S}_{Gd_2})$ in ref. 76; see ESI† for the discussion of J_3). These large exchange values have potential application in qubits as they enhance the quantum coherence required for qubit applications.[40]

A case study of magnetic anisotropy in $Dy_2@C_{59}N$ and $Tb_2@C_{59}N$

As heterofullerenes yield larger J_s and homofullerene yields relatively smaller antiferromagnetic J_s, the former is the best suited to design SMMs. The antiferromagnetic J_s in homofullerene yields diamagnetic ground states, and smaller ferromagnetic J_s observed in larger cage sizes such as C_{52} did not yield any appealing SMM characteristics. To harness SMMs in this class, heterodinuclear lanthanides with unequal m_J states were modelled. Models such as $PrEr@C_{38}$-D_{3h} yield a reasonable U_{cal} value with robust QTM quenching (*ca.* 109 cm^{-1}, see ESI†) but are not substantial to serve as a synthetic target.

Therefore, we aim to estimate the magnetic anisotropy in the $Dy_2@C_{59}N$ and $Tb_2@C_{59}N$. It is noteworthy to mention that the record-breaking magnetic anisotropy is previously achieved in $Dy_2@C_{79}N$ and $Tb_2@C_{79}N$ molecules.[44,77] The metal centre in $Dy_2@C_{59}N$ is found to interact in an η^6 fashion with the $C_{59}N$ cage, which creates a strong uniaxial anisotropy (see Fig. 1c) as a long Dy···Dy bond (3.056 Å) induces a weak ligand field in the opposite site of cage binding. Thus, the coordination can be compared with Dy^{3+}–O, which perfectly suits the oblate ground state.[91,92] The easy axis of magnetisation is found to be nearly collinear with the Dy–Dy axis with a very small angle (2.0 (1.1°) for Dy1(Dy2), Fig. S72†). The calculated g_z values of KD1 (~19.97) imply an Ising ground state for both the Dy centres (Tables S70, S71 and Fig. S71†), with the relaxation predicted to

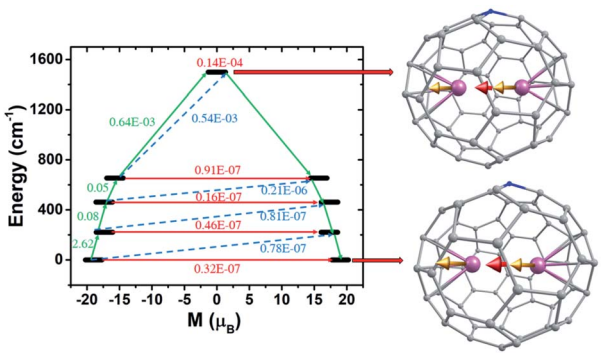

Fig. 4 The POLY_ANISO computed relaxation mechanism of $Tb_2@C_{59}N$-C_s. The anisotropy axis of the metal (represented by yellow) and radical (represented by red) centre are shown on the right. The thick black line represents the magnetic moment of KDs. The red arrows imply the QTM for ground KD and TA-QTM for higher excited KDs. The blue dotted arrows indicate a possible Orbach process. The green arrows represent the mechanism of magnetic relaxation. Colour code: Tb-blue violet, C-grey, N-blue.

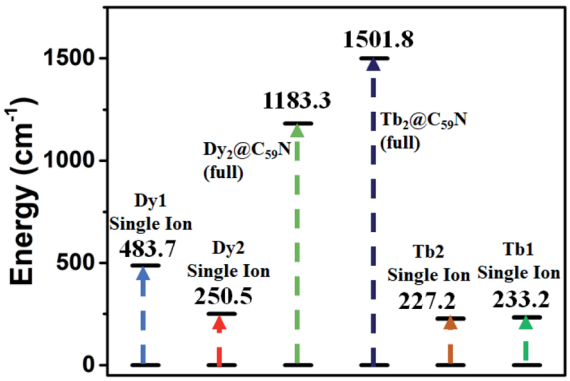

Fig. 5 Diagrammatic representation of the estimated single ion and exchange-coupled U_{cal} for $Dy_2@C_{59}N$-C_s and $Tb_2@C_{59}N$-C_s.

proceed *via* the first excited state for Dy2 ($U_{cal} = 250.5$ cm^{-1}) and third excited state for the Dy1 centre ($U_{cal} = 483.7$ cm^{-1}, Fig. S71 and Tables S70, S71†). The very large axial crystal field parameter[93] B_kq ($k = 0$, $q = 0$) compared to the non-axial crystal field parameter B_kq ($k = 0$, $q \neq 0$) suggests significant axiality for both the Dy centres in $Dy_2@C_{59}N$ (see Table S72†). Furthermore, the axial CF parameters are found to be slightly larger in $Dy_2@C_{59}N$ compared to $Dy_2@C_{79}N$, suggesting a larger axiality of the former compared to the latter.[44]

The *ab initio* calculations on $Tb_2@C_{59}N$ reveal a negligible tunnel splitting in the ground pKDs (0.025(0.013) cm^{-1} for Tb1(Tb2), see Tables S73, S74 and Fig. S73†). Further, the ground state g_z value (g_z = 17.921(17.919) for Tb1(Tb2) centre[94,95]) suggests the Ising nature of the ground state. The ground anisotropy axis of the Tb1(Tb2) centre is oriented along the pseudo C_6 axis of the hexagonal ring and nearly collinear with the Tb–Tb axis (the tilting angle becomes 0.45 and 1.50° for Tb1 and Tb2 centres, respectively, Fig. 4). However, the significant tunnel splitting (0.115 and 0.102 cm^{-1} for Tb1(Tb2), Fig. S73†) in the first excited pKDs reinforces the magnetisation relaxation *via* this state. This leads to the U_{cal} value of 227.6 and 233.2 cm^{-1} for Tb1 and Tb2 centres, respectively (see Tables S73, S74 and S70†).

To explore the mechanism of magnetisation relaxation in the exchange-coupled $Dy_2@C_{79}N$ and $Tb_2@C_{79}N$ systems, we have simulated the exchange-coupled energy spectrum using the POLY_ANISO module (see Table 1 and computational details). For the computed ground state, a large magnetic moment of *ca.* 21 and 19 μ_B for $Dy_2@C_{59}N$ and $Tb_2@C_{59}N$ respectively, was obtained (see Fig. 4 and S72†) with negligible tunnel splitting or QTM effects. The first, second, and third excited states are found to possess negligible tunnel splitting/TA-QTM, which is reflected in negligible g_x/g_y and very large g_z values (see Tables S75, S76, Fig. 4 and S72†). The magnetic moment in the fourth excited state is very small, and it results in sizeable QTM for $Dy_2@C_{59}N$ and $Tb_2@C_{59}N$. Therefore, the magnetisation relaxation for this exchange-coupled system is expected *via* the fourth excited state yielding a record-high U_{cal} value of 1183.3 and 1501.8 cm^{-1} for $Dy_2@C_{59}N$ and $Tb_2@C_{59}N$, respectively (see Fig. 4, 5, and S72†). These gigantic U_{cal} values are two times larger than $Dy_2@C_{79}N$/$Tb_2@C_{79}N$ estimates, thanks to a very large ferromagnetic exchange.[44,77] The other relaxation process due to intermolecular interactions is expected to be minimal due to confinement, which is likely to yield large T_B values. As our predictions on $Gd_2@C_{79}N$ and $Dy_2@C_{79}N$ are proved by experiments lately, with $Dy_2@C_{79}N$ yielding an attractive blocking temperature (24 K), these smaller cages, if made, could enhance T_B values even further.[40,44,47,76]

Conclusions

To this end, we have employed an array of theoretical tools in search of finding lanthanide encapsulated fullerenes with very large blocking barriers and blocking temperatures. Various ideas, such as enhancing the coupling between two lanthanide ions by bringing them close to each other in the confined space, have been tested, and the main conclusions drawn from this works are summarised below.

(i) Sourcing the large J_{Gd-Gd} exchange *via* confinement: in search of increasing the magnetic exchange (J_{Gd-Gd}) between two lanthanide ions *via* confinement, we have varied the cage size from C_{30} to C_{80} where the Gd···Gd distance ranging from 2.185 Å to 4.107 Å is observed. Here smaller cages (C_{2n}, $2n \leq 52$) yield a weaker Gd···Gd interactions with a stable $Gd_2@C_{38}$-D_{3h} complex having a record-high exchange for any 4f–4f interaction ($J_{Gd\cdots Gd} = -43.4$ cm^{-1}). A strong 4f–4f orbital overlap between two Gd^{3+} ions suggests the Gd–Gd bond formation under confinement. As the exchange is antiferromagnetic, these are not ideal for SMMs, however among hetero dilanthanide EMFs, some promising SMMs are identified.

(ii) *Ab initio* estimation of double exchange in endohedral azafullerenes: the larger cages ($Gd_2@C_{60}$ and $Gd_2@C_{80}$) lead to the formation of a two-centre-one-electron Gd–Gd bond due to the comparable energy of the highest occupied orbitals of Gd_2 and lowest unoccupied orbitals of the fullerene cage. Here we have studied $Gd_2@C_{59/79}N$ complexes where the delocalisation of the electron between two Gd centres is treated *via* a double-exchange parameter. A protocol to compute the double-exchange using *ab initio* CASSCF calculations is proposed, and this methodology yields spin Hamiltonian parameters that are in excellent agreement with experiments for $Gd_2@C_{79}N$. The application of this method in $Gd_2@C_{59}N$ unveils a massive J_{Gd-rad} exchange (J_{Gd-rad} = +869 cm^{-1}) which is two times larger than the record-high J reported for $Gd_2@C_{79}N$.

(iii) Record-high blocking barrier for $Dy_2@C_{59}N$ and $Tb_2@C_{59}N$: the huge ferromagnetic J_{Gd-rad} exchange found in the $C_{59}N$ cage quenches the QTM significantly and yields a very high U_{cal} value of 1502 cm^{-1} for $Tb_2@C_{59}N$ – the largest reported for any lanthanide EMF. This opens up the possibility of generating large magnetic anisotropy without relying on a stronger ligand field.

Computational details

All the DFT calculations have been performed using the Gaussian09 suite with the B3LYP functional.[96,97] There are several isomers with different symmetries possible for a chosen

fullerene cage. To estimate the effect of symmetry of the fullerene cage in the associated magnetic properties, we have chosen two low energy conformers of the C_{2n} ($n = 15$–24, 26, 30, 40) fullerene from http://www.nanotube.msu.edu/ and encapsulated two Gd atoms.[98] The optimisation of the resulting $Gd_2@C_{2n}$ has been performed using the UB3LYP/CSDZ(Gd), SVP (rest) methodology.[99,100] Further single point energy calculations were performed with an Ahlrichs' triple-ξ valence (TZV) basis set to obtain an excellent numerical estimate of energy/magnetic coupling.[101] A quadratic convergence SCF method was used throughout all the calculations.[102] One high spin (HS, the spin on both Gd^{3+} centres is "up") and one broken symmetry (BS, the spin on one Gd^{3+} centre is "up" and another Gd^{3+} centre is "down") configuration was used to estimate the magnetic exchange. The magnetic exchange has been calculated using the Hamiltonian $\hat{H} = -J\hat{S}_1\hat{S}_2$, where $J = \frac{E_{BS} - E_{HS}}{2S_1S_2 + S_2}$.[103,104] Additionally, we have performed AIM (atoms in molecules) analysis with the AIM2000 programme package to determine the coordination number of the Gd^{3+} ion inside the fullerene cage along with the nature of Gd–C and Gd–Gd bonds.[105]

To estimate the double exchange in $Gd_2@C_{79}N$ and $Gd_2@C_{59}N$ molecules, *ab initio* CASSCF calculations have been performed using the MOLCAS 8.4 programme package.[106] We have employed [Ln·ANO-RCC···8s7p5d3f2g1h], [C·ANO-RCC···3s2p1d] and [N·ANO-RCC···3s2p1d] contraction schemes in the basis set for Gd, C and N, respectively.[106,107] The DKH Hamiltonian was used to take into account the scaler relativistic effect.[108] The Cholesky decomposition technique was used to reduce the size of the disk space.[109] The CASSCF calculations have been performed with the CAS (15,15) active space.[90] The active space includes seven 4f orbitals from each Gd atom and one orbital for the unpaired electron. Within the active space, we have computed the energy of the $S = 13/2$, 11/2, 9/2, 7/2, 5/2 and 3/2 states with two roots while the energy of $S = 15/2$ and 1/2 states has been estimated using only one root. Further details on the computational methods are elaborated in the ESI.†

The magnetic anisotropy in the $Gd_2@C_{38}$-D_{3h} and $Gd_2@C_{52}$-D_{2d} isomer has been estimated by replacing the isotropic Gd metal centres with Dy, Er and Pr. For $Gd_2@C_{59}N$ model, anisotropic calculations were perforemd using Dy and Tb ions. The CASSCF calculations have been performed with minimal CAS(n,7) active space (n = number of 4f electrons) for Pr, Dy, Tb and Er using the MOLCAS 8.4 programme package.[106] We have computed the energies of the 21 triplets and 28 singlets of Pr^{3+}, 7 septets, 140 quintets and 195 triplets for Tb^{3+}, 21 sextets for Dy^{3+}, and 35 quartets and 112 doublets for Er^{3+} within the size of the active space. Thereafter, the computed spin-free states (7 septets, 105 quintets and 112 triplets for Tb^{3+}) have been mixed in RASSI-SO to obtain the spin–orbit coupled energies. Finally, the g tensors, QTM/TA-QTM, *etc.* of the metal centre have been computed by SINGLE_ANISO, which interfaces with the RASSI-SO. After calculating the magnetic anisotropy of the individual metal centres, they have been coupled by POLY_ANISO using the Lines model to compute the energy of the exchange-coupled system.[110] The magnetic exchange computed with the DFT and *ab initio* approach has been scaled with 5/7, 6/7, and 3/7 for Dy, Tb and Er centres, respectively, to estimate exchange coupled energy levels.

Author contributions

GR conceived the idea and SD performed all the calculations and interpret and analyse the data. Both wrote the manuscript together.

Conflicts of interest

There are no conflicts to declare.

Acknowledgements

SD would like to thank UGC for the SRF fellowship and Dr Hélène Bolvin, UPS, Toulouse for her helpful suggestions. GR would like to thank DST/SERB (CRG/2018/000430, DST/SJF/CSA03/2018-10; SB/SJF/2019–20/12; SPR/2019/001145) for funding.

Notes and references

1 R. Sessoli, D. Gatteschi, A. Caneschi and M. Novak, *Nature*, 1993, **365**, 141–143.
2 E. Moreno-Pineda, C. Godfrin, F. Balestro, W. Wernsdorfer and M. Ruben, *Chem. Soc. Rev.*, 2018, **47**, 501–513.
3 N. Ishikawa, M. Sugita, T. Ishikawa, S.-y. Koshihara and Y. Kaizu, *J. Am. Chem. Soc.*, 2003, **125**, 8694–8695.
4 A. B. Canaj, S. Dey, E. R. Martí, C. Wilson, G. Rajaraman and M. Murrie, *Angew. Chem., Int. Ed.*, 2019, **131**, 14284–14289.
5 A. B. Canaj, S. Dey, C. Wilson, O. Céspedes, G. Rajaraman and M. Murrie, *Chem. Commun.*, 2020, **56**, 12037–12040.
6 S. Dey, G. Velmurugan and G. Rajaraman, *Dalton Trans.*, 2019, **48**, 8976–8988.
7 M. S. Norre, C. Gao, S. Dey, S. K. Gupta, A. Borah, R. Murugavel, G. Rajaraman and J. Overgaard, *Inorg. Chem.*, 2019, **59**, 717–729.
8 S. Dey and G. Rajaraman, *Dalton Trans.*, 2020, **49**, 14781–14785.
9 Y. S. Ding, N. F. Chilton, R. E. Winpenny and Y. Z. Zheng, *Angew. Chem., Int. Ed.*, 2016, **55**, 16071–16074.
10 S. K. Gupta, T. Rajeshkumar, G. Rajaraman and R. Murugavel, *Chem. Sci.*, 2016, **7**, 5181–5191.
11 C. A. P. Goodwin, F. Ortu, D. Reta, N. F. Chilton and D. P. Mills, *Nature*, 2017, **548**, 439–442.
12 F.-S. Guo, B. M. Day, Y.-C. Chen, M.-L. Tong, A. Mansikkamäki and R. A. Layfield, *Science*, 2018, **362**, 1400–1403.
13 D. Reta, J. G. Kragskow and N. F. Chilton, *J. Am. Chem. Soc.*, 2021, **143**(15), 5943–5950.
14 K. R. McClain, C. A. Gould, K. Chakarawet, S. J. Teat, T. J. Groshens, J. R. Long and B. G. Harvey, *Chem. Sci.*, 2018, **9**, 8492–8503.
15 P. Evans, D. Reta, G. F. Whitehead, N. F. Chilton and D. P. Mills, *J. Am. Chem. Soc.*, 2019, **141**, 19935–19940.

16 R. Sessoli, H. L. Tsai, A. R. Schake, S. Wang, J. B. Vincent, K. Folting, D. Gatteschi, G. Christou and D. N. Hendrickson, *J. Am. Chem. Soc.*, 1993, **115**, 1804–1816.
17 V. E. Campbell, M. Tonelli, I. Cimatti, J. B. Moussy, L. Tortech, Y. J. Dappe, E. Riviere, R. Guillot, S. Delprat, R. Mattana, P. Seneor, P. Ohresser, F. Choueikani, E. Otero, F. Koprowiak, V. G. Chilkuri, N. Suaud, N. Guihery, A. Galtayries, F. Miserque, M. A. Arrio, P. Sainctavit and T. Mallah, *Nat. Commun.*, 2016, **7**, 13646.
18 L. Rosado Piquer, E. Jiménez Romero, Y. Lan, W. Wernsdorfer, G. Aromí and E. C. Sañudo, *Inorg. Chem. Front.*, 2017, **4**, 595–603.
19 C. Wäckerlin, F. Donati, A. Singha, R. Baltic, S. Rusponi, K. Diller, F. Patthey, M. Pivetta, Y. Lan and S. Klyatskaya, *Adv. Mater.*, 2016, **28**, 5195–5199.
20 V. E. Campbell, M. Tonelli, I. Cimatti, J.-B. Moussy, L. Tortech, Y. J. Dappe, E. Rivière, R. Guillot, S. Delprat and R. Mattana, *Nat. Commun.*, 2016, **7**, 1–10.
21 M. Mannini, F. Pineider, C. Danieli, F. Totti, L. Sorace, P. Sainctavit, M.-A. Arrio, E. Otero, L. Joly and J. C. Cezar, *Nature*, 2010, **468**, 417.
22 D. N. Woodruff, R. E. Winpenny and R. A. Layfield, *Chem. Rev.*, 2013, **113**, 5110–5148.
23 Y.-N. Guo, G.-F. Xu, W. Wernsdorfer, L. Ungur, Y. Guo, J. Tang, H.-J. Zhang, L. F. Chibotaru and A. K. Powell, *J. Am. Chem. Soc.*, 2011, **133**, 11948–11951.
24 F. Habib, G. Brunet, V. Vieru, I. Korobkov, L. F. Chibotaru and M. Murugesu, *J. Am. Chem. Soc.*, 2013, **135**, 13242–13245.
25 P. Evans, D. Reta, C. A. P. Goodwin, F. Ortu, N. F. Chilton and D. P. Mills, *Chem. Commun.*, 2020, **56**, 5677–5680.
26 T. Han, Y.-S. Ding, Z.-H. Li, K.-X. Yu, Y.-Q. Zhai, N. F. Chilton and Y.-Z. Zheng, *Chem. Commun.*, 2019, **55**, 7930–7933.
27 J. Long, F. Habib, P.-H. Lin, I. Korobkov, G. Enright, L. Ungur, W. Wernsdorfer, L. F. Chibotaru and M. Murugesu, *J. Am. Chem. Soc.*, 2011, **133**, 5319–5328.
28 S. K. Langley, D. P. Wielechowski, V. Vieru, N. F. Chilton, B. Moubaraki, B. F. Abrahams, L. F. Chibotaru and K. S. Murray, *Angew. Chem., Int. Ed.*, 2013, **52**, 12014–12019.
29 A. Venugopal, F. Tuna, T. P. Spaniol, L. Ungur, L. F. Chibotaru, J. Okuda and R. A. Layfield, *Chem. Commun.*, 2013, **49**, 901–903.
30 H. Tian, L. Ungur, L. Zhao, S. Ding, J. Tang and L. F. Chibotaru, *Chem.–Eur. J.*, 2018, **24**, 9928–9939.
31 A. A. Popov, S. Yang and L. Dunsch, *Chem. Rev.*, 2013, **113**, 5989–6113.
32 R. Nakanishi, J. Satoh, K. Katoh, H. Zhang, B. K. Breedlove, M. Nishijima, Y. Nakanishi, H. Omachi, H. Shinohara and M. Yamashita, *J. Am. Chem. Soc.*, 2018, **140**, 10955–10959.
33 C. H. Chen, L. Spree, E. Koutsouflakis, D. S. Krylov, F. Liu, A. Brandenburg, G. Velkos, S. Schimmel, S. M. Avdoshenko and A. Fedorov, *Adv. Sci.*, 2021, **8**, 2000777.
34 D. S. Krylov, S. Schimmel, V. Dubrovin, F. Liu, T. N. Nguyen, L. Spree, C. H. Chen, G. Velkos, C. Bulbucan and R. Westerström, *Angew. Chem., Int. Ed.*, 2020, **59**, 5756–5764.
35 T. Zuo, L. Xu, C. M. Beavers, M. M. Olmstead, W. Fu, T. D. Crawford, A. L. Balch and H. C. Dorn, *J. Am. Chem. Soc.*, 2008, **130**, 12992–12997.
36 T. Greber, A. P. Seitsonen, A. Hemmi, J. Dreiser, R. Stania, F. Matsui, M. Muntwiler, A. Popov and R. Westerström, *Phys. Rev. Mater.*, 2019, **3**, 014409.
37 C.-H. Chen, D. Krylov, S. Avdoshenko, F. Liu, L. Spree, R. Westerström, C. Bulbucan, M. Studniarek, J. Dreiser and A. Wolter, *Nanoscale*, 2018, **10**, 11287–11292.
38 S. Schimmel, Z. Sun, D. Baumann, D. Krylov, N. Samoylova, A. Popov, B. Büchner and C. Hess, *Beilstein J. Nanotechnol.*, 2017, **8**, 1127–1134.
39 V. Martinez, B. Karadeniz, N. Biliškov, I. Lončarić, S. Muratović, D. Zilic, S. M. Avdoshenko, M. Roslova, A. A. Popov and K. Uzarevic, *Chem. Mater.*, 2020, **32**, 10628–10640.
40 Z. Hu, B. W. Dong, Z. Liu, J. J. Liu, J. Su, C. Yu, J. Xiong, D. E. Shi, Y. Wang, B. W. Wang, A. Ardavan, Z. Shi, S. D. Jiang and S. Gao, *J. Am. Chem. Soc.*, 2018, **140**, 1123–1130.
41 J. D. Rinehart, M. Fang, W. J. Evans and J. R. Long, *J. Am. Chem. Soc.*, 2011, **133**, 14236–14239.
42 V. Vieru, N. Iwahara, L. Ungur and L. F. Chibotaru, *Sci. Rep.*, 2016, **6**, 1–8.
43 S. Demir, M. I. Gonzalez, L. E. Darago, W. J. Evans and J. R. Long, *Nat. Commun.*, 2017, **8**, 1–9.
44 M. K. Singh, N. Yadav and G. Rajaraman, *Chem. Commun.*, 2015, **51**, 17732–17735.
45 M. K. Singh and G. Rajaraman, *Chem. Commun.*, 2016, **52**, 14047–14050.
46 Z. Hu, B.-W. Dong, Z. Liu, J.-J. Liu, J. Su, C. Yu, J. Xiong, D.-E. Shi, Y. Wang and B.-W. Wang, *J. Am. Chem. Soc.*, 2018, **140**, 1123–1130.
47 F. Liu, D. S. Krylov, L. Spree, S. M. Avdoshenko, N. A. Samoylova, M. Rosenkranz, A. Kostanyan, T. Greber, A. U. B. Wolter, B. Buchner and A. A. Popov, *Nat. Commun.*, 2017, **8**, 16098.
48 G. Velkos, D. S. Krylov, K. Kirkpatrick, X. Liu, L. Spree, A. U. B. Wolter, B. Buchner, H. C. Dorn and A. A. Popov, *Chem. Commun.*, 2018, **54**, 2902–2905.
49 Y. Wang, J. Xiong, J. Su, Z. Hu, F. Ma, R. Sun, X. Tan, H.-L. Sun, B.-W. Wang and Z. Shi, *Nanoscale*, 2020, **12**, 11130–11135.
50 C. A. Gould, L. E. Darago, M. I. Gonzalez, S. Demir and J. R. Long, *Angew. Chem., Int. Ed.*, 2017, **129**, 10237–10241.
51 S. Demir, I.-R. Jeon, J. R. Long and T. D. Harris, *Coord. Chem. Rev.*, 2015, **289**, 149–176.
52 K. R. Meihaus, J. F. Corbey, M. Fang, J. W. Ziller, J. R. Long and W. J. Evans, *Inorg. Chem.*, 2014, **53**, 3099–3107.
53 S. Demir, J. M. Zadrozny, M. Nippe and J. R. Long, *J. Am. Chem. Soc.*, 2012, **134**, 18546–18549.
54 J. D. Rinehart, M. Fang, W. J. Evans and J. R. Long, *Nat. Chem.*, 2011, **3**, 538–542.
55 C. A. Gould, E. Mu, V. Vieru, L. E. Darago, K. Chakarawet, M. I. Gonzalez, S. Demir and J. R. Long, *J. Am. Chem. Soc.*, 2020, **142**, 21197–21209.

56 P. Sharma, D. R. Pahls, B. L. Ramirez, C. C. Lu and L. Gagliardi, *Inorg. Chem.*, 2019, **58**, 10139–10147.
57 S. X. Hu, E. Lu and S. T. Liddle, *Dalton Trans.*, 2019, **48**, 12867–12879.
58 C. Jones, C. Schulten, R. P. Rose, A. Stasch, S. Aldridge, W. D. Woodul, K. S. Murray, B. Moubaraki, M. Brynda, G. La Macchia and L. Gagliardi, *Angew. Chem., Int. Ed.*, 2009, **48**, 7406–7410.
59 A. Khong, H. A. Jiménez-Vázquez, M. Saunders, R. J. Cross, J. Laskin, T. Peres, C. Lifshitz, R. Strongin and A. B. Smith, *J. Am. Chem. Soc.*, 1998, **120**, 6380–6383.
60 R.-F. Peng, S.-J. Chu, Y.-M. Huang, H.-J. Yu, T.-S. Wang, B. Jin, Y.-B. Fu and C.-R. Wang, *J. Mater. Chem.*, 2009, **19**, 3602–3605.
61 T. Yu. Nikolaienko, E. S. Kryachko and G. A. Dolgonos, *J. Comput. Chem.*, 2018, **39**, 1090–1102.
62 E. Cerpa, A. Krapp, R. Flores-Moreno, K. J. Donald and G. Merino, *Chem.–Eur. J.*, 2009, **15**, 1985–1990.
63 S. Jalife, S. Mondal, J. L. Cabellos, S. Pan, M. A. Mendez-Rojas, I. Fernández, G. Frenking and G. Merino, *ChemistrySelect*, 2016, **1**, 2405–2408.
64 K. Li, H. Lian and R. V. Deun, *J. Lumin.*, 2018, **198**, 155–162.
65 M. Parthey and M. Kaupp, *Chem. Soc. Rev.*, 2014, **43**, 5067–5088.
66 F. Liu, L. Spree, D. S. Krylov, G. Velkos, S. M. Avdoshenko and A. A. Popov, *Acc. Chem. Res.*, 2019, **52**, 2981–2993.
67 X. Cao and M. Dolg, *Theor. Chem. Acc.*, 2002, **108**, 143–149.
68 S. Ghosh, S. K. Singh, S. Tewary and G. Rajaraman, *Dalton Trans.*, 2013, **42**, 16490–16493.
69 B. Bechlars, D. M. D'alessandro, D. M. Jenkins, A. T. Iavarone, S. D. Glover, C. P. Kubiak and J. R. Long, *Nat. Chem.*, 2010, **2**, 362–368.
70 O. Kahn, *Molecular Magnetism*, VCH Publishers, Inc., USA, 1993.
71 A. A. Popov, *Curr. Opin. Electrochem.*, 2018, **8**, 73–80.
72 F. Liu, D. S. Krylov, L. Spree, S. M. Avdoshenko, N. A. Samoylova, M. Rosenkranz, A. Kostanyan, T. Greber, A. U. Wolter and B. Büchner, *Nat. Commun.*, 2017, **8**, 1–9.
73 A. A. Popov, S. M. Avdoshenko, A. M. Pendás and L. Dunsch, *Chem. Commun.*, 2012, **48**, 8031–8050.
74 L. Bao, M. Chen, C. Pan, T. Yamaguchi, T. Kato, M. M. Olmstead, A. L. Balch, T. Akasaka and X. Lu, *Angew. Chem., Int. Ed.*, 2016, **128**, 4314–4318.
75 F. Liu, G. Velkos, D. S. Krylov, L. Spree, M. Zalibera, R. Ray, N. A. Samoylova, C.-H. Chen, M. Rosenkranz and S. Schiemenz, *Nat. Commun.*, 2019, **10**, 1–11.
76 G. Velkos, D. Krylov, K. Kirkpatrick, X. Liu, L. Spree, A. Wolter, B. Büchner, H. Dorn and A. Popov, *Chem. Commun.*, 2018, **54**, 2902–2905.
77 G. Velkos, D. S. Krylov, K. Kirkpatrick, L. Spree, V. Dubrovin, B. Büchner, S. M. Avdoshenko, V. Bezmelnitsyn, S. Davis and P. Faust, *Angew. Chem., Int. Ed.*, 2019, **58**, 5891–5896.
78 A. Kostanyan, R. Westerström, D. Kunhardt, B. Büchner, A. A. Popov and T. Greber, *Phys. Rev. B: Condens. Matter Mater. Phys.*, 2020, **101**, 134429.
79 W. Fu, J. Zhang, T. Fuhrer, H. Champion, K. Furukawa, T. Kato, J. E. Mahaney, B. G. Burke, K. A. Williams and K. Walker, *J. Am. Chem. Soc.*, 2011, **133**, 9741–9750.
80 T. Kaneko, Y. Li, S. Nishigaki and R. Hatakeyama, *J. Am. Chem. Soc.*, 2008, **130**, 2714–2715.
81 S. Ostrowski, P. Garnuszek and J. C. Dobrowolski, *Spectrochim. Acta Mol. Biomol. Spectrosc.*, 2020, **231**, 117791.
82 C. Brown, L. Cristofolini, K. Kordatos, K. Prassides, C. Bellavia, R. Gonzalez, M. Keshavarz-K, F. Wudl, A. Cheetham and J. Zhang, *Chem. Mater.*, 1996, **8**, 2548–2550.
83 W. Si, X. Zhang, N. Asao, Y. Yamamoto and T. Jin, *Chem. Commun.*, 2015, **51**, 6392–6394.
84 K. Hedberg, L. Hedberg, D. S. Bethune, C. Brown, H. Dorn, R. D. Johnson and M. de Vries, *Science*, 1991, **254**, 410–412.
85 R. D. Johnson, C. S. Yannoni, H. C. Dorn, J. R. Salem and D. S. Bethune, *Science*, 1992, **255**, 1235–1238.
86 Y.-F. Yang and L. S. Cederbaum, *Phys. Chem. Chem. Phys.*, 2021, **23**, 11837–11843.
87 K. Prassides, M. Keshavarz-K, J. C. Hummelen, W. Andreoni, P. Giannozzi, E. Beer, C. Bellavia, L. Cristofolini, R. González and A. Lappas, *Science*, 1996, **271**, 1833–1835.
88 W. Andreoni, A. Curioni, K. Holczer, K. Prassides, M. Keshavarz-K, J.-C. Hummelen and F. Wudl, *J. Am. Chem. Soc.*, 1996, **118**, 11335–11336.
89 M. Keshavarz-K, R. González, R. G. Hicks, G. Srdanov, V. I. Srdanov, T. G. Collins, J. C. Hummelen, C. Bellavia-Lund, J. Pavlovich and F. Wudl, *Nature*, 1996, **383**, 147–150.
90 F. Cimpoesu, B. Frecus, C. I. Oprea, H. Ramanantoanina, W. Urland and C. Daul, *Mol. Phys.*, 2015, **113**, 1712–1727.
91 L. Ungur, M. Thewissen, J.-P. Costes, W. Wernsdorfer and L. F. Chibotaru, *Inorg. Chem.*, 2013, **52**, 6328–6337.
92 L. Ungur and L. F. Chibotaru, *Phys. Chem. Chem. Phys.*, 2011, **13**, 20086–20090.
93 L. F. Chibotaru and L. Ungur, *J. Chem. Phys.*, 2012, **137**, 064112.
94 J. Griffith, *Phys. Rev.*, 1963, **132**, 316.
95 J. S. Griffith, *The theory of transition-metal ions*, Cambridge University Press, 1964.
96 M. J. Frisch, G. W. Trucks, H. B. Schlegel, G. E. Scuseria, M. A. Robb, J. R. Cheeseman, G. Scalmani, V. Barone, B. Mennucci, G. A. Petersson, H. Nakatsuji, M. Caricato, X. Li, H. P. Hratchian, A. F. Izmaylov, J. Bloino, G. Zheng, J. L. Sonnenberg, M. Hada, M. Ehara, K. Toyota, R. Fukuda, J. Hasegawa, M. Ishida, T. Nakajima, Y. Honda, O. Kitao, H. Nakai, T. Vreven, J. A. Montgomery Jr, J. E. Peralta, F. Ogliaro, M. Bearpark, J. J. Heyd, E. Brothers, K. N. Kudin, V. N. Staroverov, R. Kobayashi, J. Normand, K. Raghavachari, A. Rendell, J. C. Burant, S. S. Iyengar, J. Tomasi, M. Cossi, N. Rega, J. M. Millam, M. Klene, J. E. Knox, J. B. Cross, V. Bakken, C. Adamo, J. Jaramillo, R. Gomperts, R. E. Stratmann, O. Yazyev, A. J. Austin, R. Cammi, C. Pomelli, J. W. Ochterski, R. L. Martin, K. Morokuma, V. G. Zakrzewski, G. A. Voth, P. Salvador, J. J. Dannenberg, S. Dapprich, A. D. Daniels, O. Farkas, J. B. Foresman, J. V. Ortiz, J. Cioslowski and

D. J. Fox, *Gaussian 09, Revision A.02*, Gaussian, Inc., Wallingford CT, 2009.
97 A. D. Beck, *J. Chem. Phys.*, 1993, **98**, 1372–1377.
98 D. Tománek, *Guide through the nanocarbon jungle*, 2014.
99 T. R. Cundari and W. J. Stevens, *J. Chem. Phys.*, 1993, **98**, 5555–5565.
100 F. Weigend and R. Ahlrichs, *Phys. Chem. Chem. Phys.*, 2005, **7**, 3297–3305.
101 A. Schäfer, H. Horn and R. Ahlrichs, *J. Chem. Phys.*, 1992, **97**, 2571–2577.
102 C. Ögretir and I. G. Csizmadia, *Computational advances in organic chemistry: molecular structure and reactivity*, Springer Science & Business Media, 2012.
103 E. Ruiz, J. Cano, S. Alvarez and P. Alemany, *J. Comput. Chem.*, 1999, **20**, 1391–1400.
104 L. Noodleman, *J. Chem. Phys.*, 1981, **74**, 5737–5743.
105 F. Biegler-König and J. Schönbohm, *J. Comput. Chem.*, 2002, **23**, 1489–1494.
106 F. Aquilante, J. Autschbach, R. K. Carlson, L. F. Chibotaru, M. G. Delcey, L. De Vico, I. F. Galván, N. Ferré, L. M. Frutos and L. Gagliardi, *J. Comput. Chem.*, 2016, **37**, 506–541.
107 B. O. Roos, V. Veryazov and P.-O. Widmark, *Theor. Chem. Acc.*, 2004, **111**, 345–351.
108 M. Reiher, *Theor. Chem. Acc.*, 2006, **116**, 241–252.
109 F. Aquilante, P.-Å. Malmqvist, T. B. Pedersen, A. Ghosh and B. O. Roos, *J. Chem. Theory Comput.*, 2008, **4**, 694–702.
110 M. Lines, *J. Chem. Phys.*, 1971, **55**, 2977–2984.